Korean J. Chem. Eng., 34(5), 1346-1357 (2017)
DOI: 10.1007/s11814-017-0026-0

pISSN: 0256-1115
eISSN: 1975-7220

CO_2/O_2-oxidative dehydrogenation of ethane to ethylene over highly dispersed vanadium oxide on MgO-promoted sulfated-zirconia nanocatalyst: Effect of sulfation on catalytic properties and performance

Parisa Taghavinezhad*,, Mohammad Haghighi*,**,†, and Reza Alizadeh*,****

*Chemical Engineering Faculty, Sahand University of Technology, P. O. Box 51335-1996, Sahand New Town, Tabriz, Iran
**Reactor and Catalysis Research Center (RCRC), Sahand University of Technology,
P. O. Box 51335-1996, Sahand New Town, Tabriz, Iran
(*Received 20 November 2016 • accepted 6 February 2017*)

Abstract−The ZrO_2 was treated by various molarities of H_2SO_4 solution (0, 0.5, 1 and 2) then mixed by MgO and impregnated with 5 wt% of V_2O_5. The synthesized catalysts were characterized by XRD, FESEM, PSD, EDX, BET and FTIR techniques. According to the results obtained by characterization studies, the modification of MgO-ZrO_2 support by various molarities of H_2SO_4 solution had a great impact on the crystallinity, morphology and functional groups of prepared nanocatalysts. On the other hand, the catalytic activity of synthesized nanocatalysts in the oxidative dehydrogenation of ethane to ethylene is affected by the sulfur content on the support. The crystalline structures of MgO and ZrO_2 were confirmed by XRD analysis. The crystallinity of tetragonal ZrO_2 was decreased by increasing H_2SO_4 molarity used in ZrO_2 (Sx) synthesising. The highest catalytic performance and ethylene productivity (C_2H_4 yield of 48% and ethane conversion of 79% at 700 °C) were obtained on the V_2O_5/MgO-ZrO_2 (S1) nanocatalyst. This could be related to the superior acid-base property, smaller particles, better dispersion of active phase and uniform morphology of V_2O_5/MgO-ZrO_2 (S1).

Keywords: Impregnation, Precipitation, V_2O_5/MgO-ZrO_2, Dehydrogenation, Ethane, Ethylene

INTRODUCTION

Oxidative dehydrogenation (ODH) of alkanes is an alternative route for the production of olefins [1-3]. Restrictions such as high energy input, coke formation and catalysis deactivation limit the utilization of traditional ways of dehydrogenation of alkanes. The petrochemical industry need for the olefins has increased, making it essential to find an economic and simple route for the production of olefins [4-6]. The catalysts used in ODH should have specifications that impede the formation of CO_2 and CO [7-9]. Among the variety of supported metal oxides applied for ODH, the vanadium-based oxide showed highest activity and stability [10,11]. However Cr_2O_3 based catalysts showed comparative performance with vanadium based catalysts; the formation of nanocrystalline Cr_2O_3 and aggregates reduces the chromium surface density and lowers the active sites needed for ODH process [12]. According to the literature data, the unsupported V_2O_5 exhibits lower selectivity to the ethylene (18-31%) compared to the supported one (29-90%). This conclusion implies that the strong interaction between the active phase and the support leads to the formation of different active sites, which promotes the dehydrogenation reaction [13-15]. The V_2O_5 atom consists of three types of oxygen. 1- O (a): bonded to one vanadium atom via double bond. 2- O (b): connected to two V atoms through bonds with 1.78 Å lengths. 3- O (c): linked to three vanadium atoms with higher bond length compared to V-O (b). Two V-O (c) bonds have the 1.78 Å and the length of the other V-O (c) bond measured 2.02 Å [16]. The simultaneous presence of V^{+4} and V^{+5} ions in the vanadium supported catalysts is believed to support the selective oxidation of ethane to the ethylene via a redox process [17].

Using the perfect support is important as it affects the active phase dispersion, reactivity, accessibility and acidity [18-20]. On the other hand, the mass and heat transfer on the catalysts are directly related to the material used in the support [21-23]. It is believed that the nature of support could be altering the V-O-S bond (where support is denoted by S), and consequently, the ODH performance of catalysts. According to Lopez-Nieto and coworkers [24], the existence of a balance between reducibility and the acid-base character is required for the ODH active sites.

The discernment that sulfated metal oxides, especially sulfated zirconia, possess an activity for hydrocarbon conversion that oversteps most or all acidic zeolite catalysts has concentrated great interest in these materials. Contrary to the extensive studies carried out, the nature of acid sites of sulfated zirconia is argumentative [25,26]. The application of such an acidic support might precede the ODH process on the way which leads to the formation of large amount of CO or CO_2 and would lead to carbon deposition on the catalyst surface. On the contrary, MgO is known as a basic support that accelerates olefin desorption and prevents the side reactions. The initial activity of MgO for ODH reaction is high due to the existence of enough oxygen capacity, but the oxygen mobility of MgO is low. ZrO_2 has lower oxygen capacity compared to MgO,

†To whom correspondence should be addressed.
E-mail: haghighi@sut.ac.ir

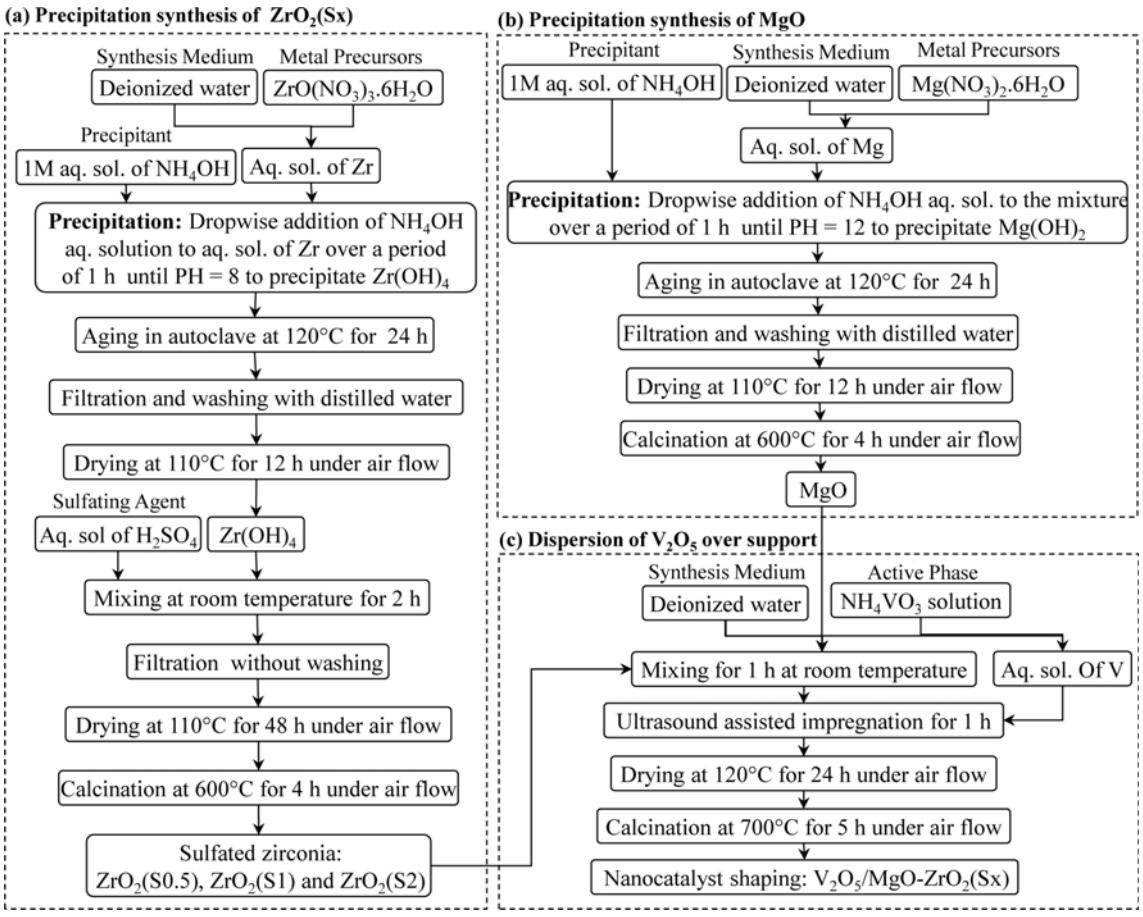

Fig. 1. Dispersion of V_2O_5 over MgO-promoted sulfated-zirconia.

but has the higher oxygen mobility [27]. According to what was mentioned above, we have proposed that MgO-ZrO_2 (Sx) supported V_2O_5 has superior activity to the ODH of ethane by CO_2. To the best of over knowledge, there is not any publication in the field of ethane ODH using MgO-ZrO_2 (Sx) composites as V_2O_5 support. To make this assumption, at the first step, MgO and ZrO_2 were prepared by precipitation methods. Then, sulfated zirconia was prepared by different molarities of H_2SO_4 solution. V_2O_5 was deposited over the supports by a wet impregnation method. The prepared catalysts were characterized by XRD, FESEM, EDX, BET, PSD and FTIR analysis. The catalytic activity of synthesized catalysts was investigated for the oxidative dehydrogenation of ethane to ethylene under atmospheric pressure employing CO_2 as a soft oxidant and a mixture of CO_2 and O_2 And the results of these two conditions were compared.

MATERIALS AND METHODS

1. Materials

Mg $(NO_3)_2{\cdot}6H_2O$ and ZrO $(NO_3)_2{\cdot}6H_2O$ (Merck) were used as support precursors. NH_4VO_3 was used as active phase precursor and was purchased from Aldrich Company. H_2SO_4 was used as sulfating agent and NH_4OH was applied to control the pH of the solutions. These materials were used as received and were not purified further. C_2H_6 (99.9%), CO_2 (99.99%), air (99.999%) and N_2 (99.9995%) were all high purity and were purchased from Technical Gas Services in Ajman, UAE.

2. Nanocatalysts Preparation and Procedures

Fig. 1 illustrates schematically the synthesis procedure used for the preparation of V_2O_5/MgO-ZrO_2 (Sx) nanocatalysts with various molarities of H_2SO_4. The required amount of Mg $(NO_3)_2{\cdot}6H_2O$ was dissolved in deionized water and stirred at room temperature. The ammonia was added dropwise to the stirring solution until the pH level reached 12. The mother solution was transferred into a Teflon-lined stainless steel autoclave and was maintained at 120 °C for 24 h. The aged solution was filtered and washed three times with cold deionized water, dried at 120 °C for 24 h and finally calcined at 600 °C for 4 h. For the preparation of sulfated zirconia the precursor salt, $ZrO(NO_3)_2{\cdot}6H_2O$ was dissolved in distilled water and aqueous ammonia was added until the pH level of the solution reached 8. The resultant gel was aged in the autoclave at 120 °C for 24 h. The solid product after filtration and washing, dried at 120 °C for 24 h. Required amounts of hydrous zirconia were dissolved in the mixture of distilled water and appropriate volume of H_2SO_4 (0.5, 1 and 2 M). This solution was mixed at room temperature for 2 h and afterwards filtered without washing, then it was dried at 120 °C for 48 h, and finally calcined at 600 °C. The obtained sulfated zirconia solid powders denoted as ZrO_2 (Sx), where x is

the molarity of applied H_2SO_4 solution. At the final steps, the required amounts of MgO and ZrO_2 (Sx) were dissolved in distilled water and stirred for 1 h, afterwards vanadium precursor was impregnated; then all samples were dried and calcined at 700 °C.

The reaction pathway shown in Fig. 2 has been proposed to the formation of sulfated zirconia. It seems that the formation of ZrO_2 (Sx) consists of two steps. In the first step, superficial hydroxyl groups react with the adsorbed sulfur groups. According to this mechanism reaction (1) takes place during the stirring of a solution consisting of sulfuric acid and Zr $(OH)_4$.

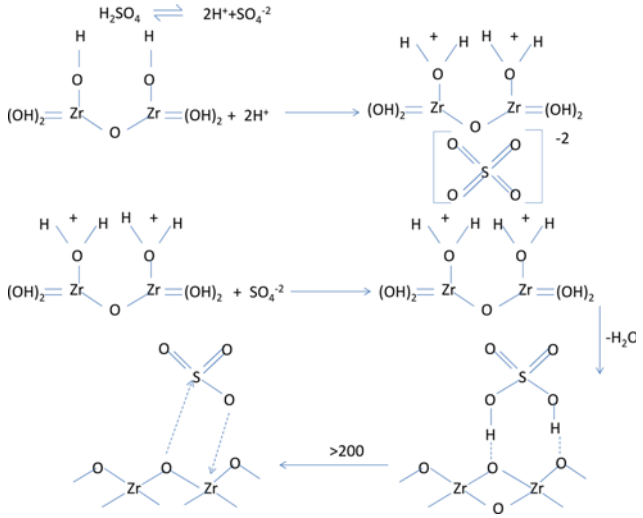

Fig. 2. Reaction pathway for sulfidation of ZrO_2.

$$Zr(OH)_{4n} + xH_2SO_4 \leftrightarrow Zr(OH)_{4n-2x}(SO_4)_x + 2xH_2O \quad (1)$$

In detail, at the above reaction, protons are attracted to the zirconia hydroxide, and then sulfur anions get ensnared at the ionized surface of Zr $(OH)_4$. First water molecules desorb during drying step.

The second stage of reaction occurs during calcinations of Zr $(OH)_4$ which is treated by sulfuric acid.

$$Zr(OH)_{4n-2x}(SO_4)_x \rightarrow ZrO_{4n-x}(SO_4)_x + (2n-x)H_2O \quad (2)$$

This mechanism explains the properties associated with the sulfated zirconia. The high content of tetragonal phase and higher surface area are the specification of sulfated material due to the presence of SO_4^{-2} anion. This mechanism is consistent with ones proposed by Chen et al. [28]. However, the nature of acid sites of sulfated zirconia is under debate, but according to the refs. [29,30] incorporation of sulfated anions increases the number and the potency of acid sites. Arata and coworkers [31] suggested a mechanism for the formation of sulfated zirconia that in addition to the Lewis acid site, Brönsted sites also detectable. According to the Arata and coworkers model, the existence of sulfur anion is responsible for the formation of Lewis sites and the reaction of water with the adsorbed sulfur species generates Brönsted acid sites [32]. Mort-

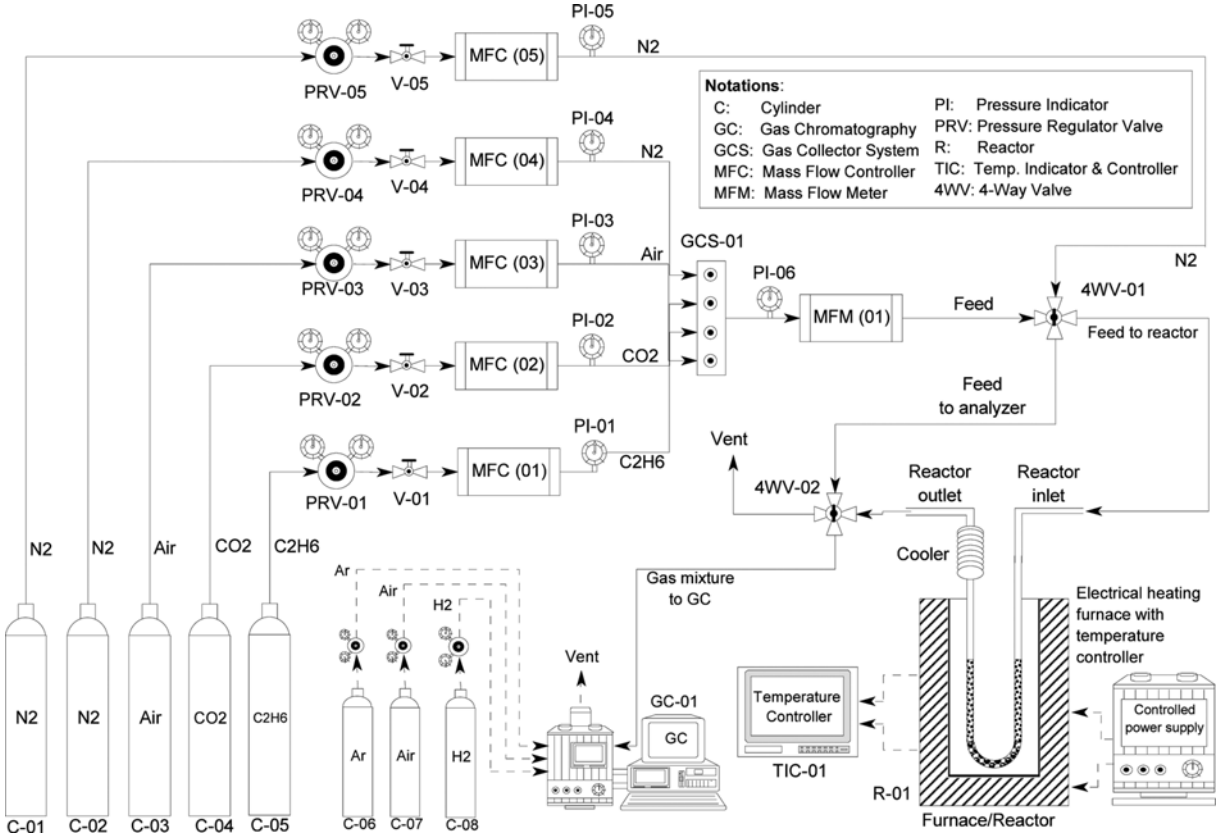

Fig. 3. Experimental setup for testing of catalytic performance of synthesized nanocatalysts used in oxidative dehydrogenation of ethane to ethylene by carbon dioxide and air.

erra et al. [33] stated that the amount of Brönsted sites depended on to the degree of dehydration of catalysis. As a result, the Brönsted acid sites are formed due to remaining water on the catalysis. However, it is not clear that Lewis or Brönsted acid sites are suitable for ODH process, but Marta et al. [34] stated that Brönsted and or Lewis acid sites lowers the olefins selectivity due to the over oxidation of ethylene. So the drying of catalysts for long time (48 h) and calcinations of catalyst at higher temperature leads to optimization of acid site's amount.

3. Nanocatalysts Characterization

Powder X-ray diffraction (XRD) analysis was performed to assess structural identification of the nanocatalysts. The XRD patterns were recorded on a Siemens diffractometer D5000 with monochromatized Cu-K radiation at 40 kV and 30 mA and a scanning angle (2θ) range of 20 to 90° and scanning rate of 0.02°/s. The phase identification was made with comparison to Joint Committee on Powder Diffraction Standards (JCPDSs). Microstructure, particle size distribution, morphology and surface particle size distribution of nanocatalysts were examined by field emission scanning electron microscopy (VEGA\\TESCAN, BSE DETECTOR). The specific surface area (BET) of nanocatalysts was determined by N_2 adsorption and desorption isotherms obtained at 77 K using a Quantachrome ChemBET-3000. Infrared analysis of the nanocatalyst was with a UNICAM 4600 FTIR spectroscope addressing surface functional groups in the range of 400-4,000 cm^{-1} wave numbers. EDX analysis was applied by VEGA\\TESCAN, BSE DETECTOR for elemental analysis.

4. Nanocatalyst Performance Test

Oxidative dehydrogenation of ethane was conducted at atmospheric pressure in a 6 mm i.d and 200 mm length U-shape quartz tube packed bed reactor which was loaded with 500 mg of nanocatalyst. To attain the isothermal condition and preheat the reactant gas, the particles of catalysts were diluted with quartz sand. The reactor configuration is shown schematically in Fig. 3. Before feeding, to enhance the catalyst oxygen capacity and eliminate water or inorganic compounds existing on the surface of catalyst, a flow of dry air (consist of <2.5 ppm H_2O) passed through the catalyst bed at T=600 °C for approximately 0.5 h. Experiments were performed at temperatures ranging from 600 to 700 °C. A mixture of carbon dioxide, ethane and nitrogen (feed) at a $CO_2/C_2H_6/N_2$=4/1/5 ratio was supplied through mass flow controllers (Beijing Sevenstar Electronics Co., Ltd.) to the nanocatalyst bed at the specified reaction condition. To investigate the effect of O_2 addition on the catalytic performance, in addition to the flow of feed gas a flow of air (in the ratio of feed/air=87/13) passed through the catalyst bed at a rate of 75 cc/min. Compositions of feed and reactor effluent gas were monitored by a gas chromatograph (GC Chrom, Teif Gostar Faraz, Iran) equipped with a flame ionization detector (FID), a thermal conductivity detector (TCD), a methanizer and a Carboxen-1000 column (Agilent Co.).

RESULTS AND DISCUSSION

1. Nanocatalyst Characterization

1-1. XRD Analysis

Fig. 4 depicts the XRD patterns of synthesized V_2O_5/MgO-ZrO_2 S(x) nanocatalysts with various concentrations of sulfating agent. According to the JCPDS files (01-077-2364) the characteristic peaks related to MgO cubic phase are observed at 2θ=37.0, 43.0, 62.4, 74.8 and 78.7° in all samples. The results illustrated in the figure reveal that V_2O_5/MgO-ZrO_2 (S0) consists of both tetragonal phase and monoclinic one. Recently, Deshmane et al. [35] studied the formation of zirconia at various calcination temperatures. They concluded that heat treatment of Zr $(OH)_4$ at 600 °C leads to the formation of a mixture of tetragonal (52%) and monoclinic phases (48%) of ZrO_2. The sulfidation of ZrO_2 enhances the tetragonal phase contribution. However, the calcination of sulfated zirconia at 600 °C leads to the removal of most of the sulfate anions, but the interaction of remaining SO_4^{-2} with zirconia is reinforced. This indicates that the presence of sulfate groups does stabilize the tetragonal structure of zirconia, probably due to the strong interactions between the sulfate group and ZrO_2. As can be seen from Fig. 4, by

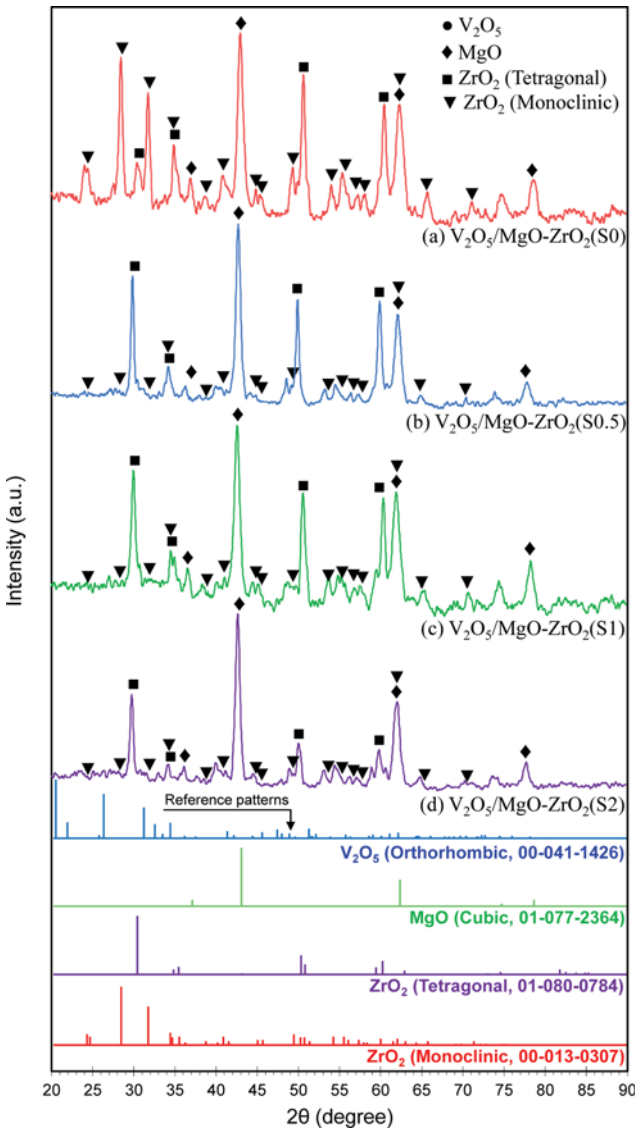

Fig. 4. XRD patterns of synthesized V_2O_5/MgO-ZrO_2 nanocatalysts: (a) V_2O_5/MgO-ZrO_2(S0), (b) V_2O_5/MgO-ZrO_2(S0.5), (c) V_2O_5/MgO-ZrO_2(S1), and (d) V_2O_5/MgO-ZrO_2(S2).

increasing the concentration of sulfating agent utilized in ZrO_2 (Sx) preparation, the intensity of tetragonal phase decreases and the structure of catalysts is gradually deformed from crystallite to amorphous. It seems that these interactions are suppressing or postponing the phase transition. It is well known that the tetragonal phase of zirconia is more active and stable in the ethane ODH. The presence of tetragonal phase of zirconia decreased the required activation energy for the reaction [36,37]. No characteristic peaks related to V_2O_5 were detected, probably due to high dispersion or small crystallites of vanadium over the supports in the case of magnesia supported vanadium oxide; it is believed that the formation of magnesia vanadate phase reduces the catalysis selectivity toward ethylene [34]. Hence this phase was not formed in any of the samples; the acceptable selectivity for all catalysts is anticipated.

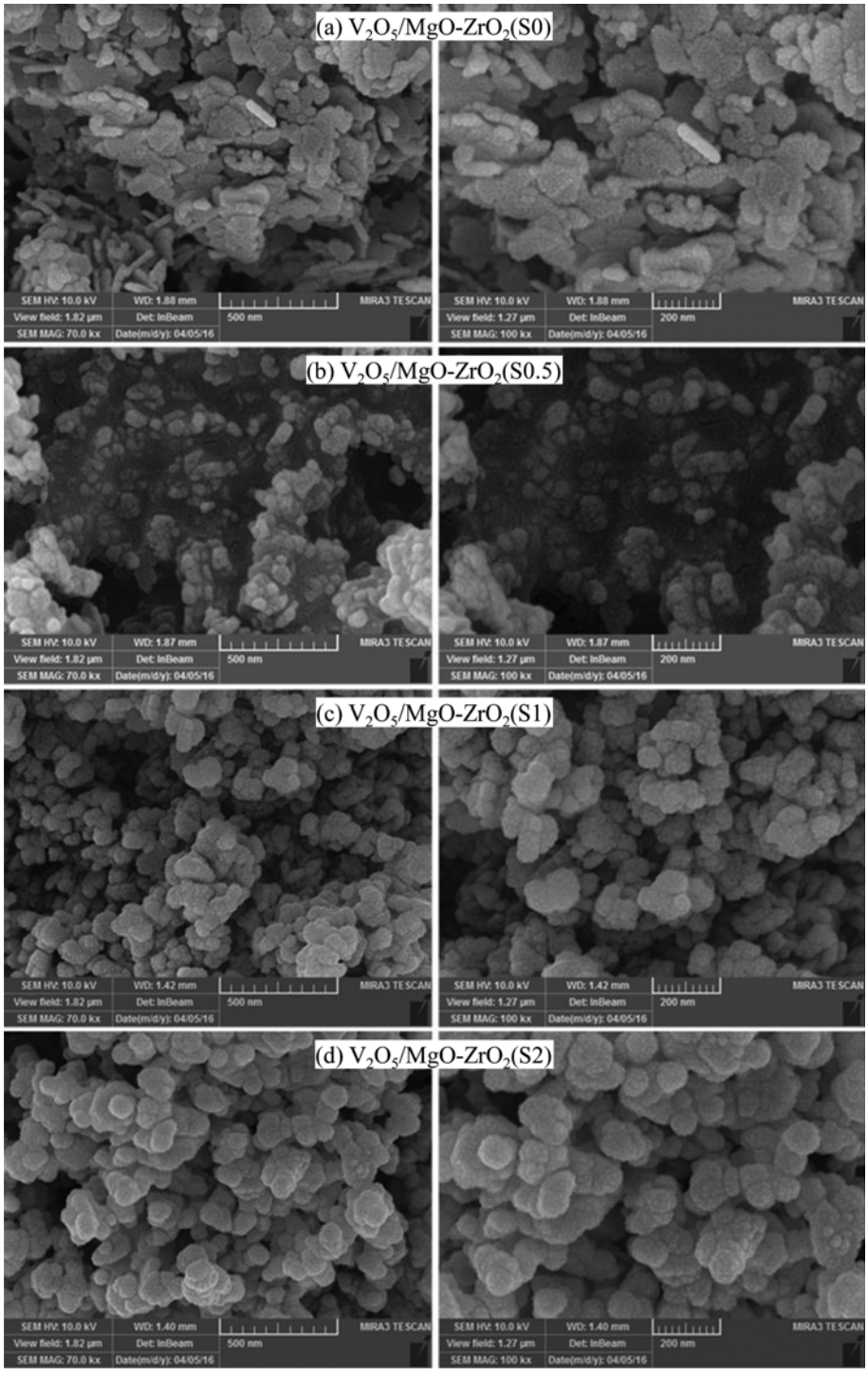

Fig. 5. FESEM images of synthesized V_2O_5/MgO-ZrO_2 nanocatalysts: (a) V_2O_5/MgO-ZrO_2(S0), (b) V_2O_5/MgO-ZrO_2(S0.5), (c) V_2O_5/MgO-ZrO_2(S1), and (d) V_2O_5/MgO-ZrO_2(S2).

1-2. FESEM Analysis

The particle morphology of nanocatalysts is shown in Fig. 5. Large amount of agglomerate observed on the surface of V_2O_5/MgO-ZrO_2 (S0) nanocatalysts causes the formation of structure with fewer interparticle voids and pores and reduces the surface area of catalysis. Also, this could be related to the formation of more intense crystalline structure of this nanocatalyst. Comparing the structure of V_2O_5/MgO-ZrO_2 (S0) and V_2O_5/MgO-ZrO_2 (S0.5) reveals that introduction of sulfur anion on the support alters the morphology of nanocatalyst from leaf shape to the nearly spherical. This observation is more obvious in the case of V_2O_5/MgO-ZrO_2 (S1) in which more uniform and approximately more spherical structures are formed. It could be concluded that variation of sulfating agent concentration in the synthesising of nanocatalysts has the ability to control the surface particle energy. From Fig. 5, by increasing sulfating agent concentration, the particle size is reduced and reaches the minimum amount at V_2O_5/MgO-ZrO_2 (S1) nanocatalyst. By increasing it even more, the particle size increases, but uniformity of catalysts remains unchanged.

Thus, the smaller particle size of V_2O_5/MgO-ZrO_2 (S1) caused a better catalytic performance for this nanocatalyst due to availability of more active sites for ODH reaction. To investigate more precision, Image-J software was applied to calculate the particle size distribution of V_2O_5/MgO-ZrO_2 (S1) nanocatalysts, and results are shown in Fig. 6. According to the results, the V_2O_5/MgO-ZrO_2 (S1) has narrow particle size distribution; and the minimum size of 23.2 nm, maximum of 105.4 nm and the average size of 63.644 nm were calculated for this nanocatalyst. More than 70% of V_2O_5/MgO-ZrO_2 (S1) particles are distributed in the range of particles less than 80 nm.

1-3. EDX Analysis

The prepared nanocatalysts were analyzed by EDX to determine the surface composition of elements present in each catalyst. The elemental compositions of species are shown in Fig. 7. All the materials used in the preparation of nanocatalysts (Zr, S, Mg and V) can be observed in the EDX dot mapping pictures. These results proved the presence of V species as active phase which are not detected in XRD patterns. As can be seen, V is dispersed uniformly on the surface of all catalysts, and the ensembles related to V spices are not detected. This indicates that Mg-ZrO_2 (Sx) is a very good support for dispersion of V_2O_5. On the other hand, this proved the success of precipitation method used for the synthesis of supports. Our result is in good agreement with XRD analysis that no peaks related to V_2O_5 are detected. V_2O_5/MgO-ZrO_2 (Sx) catalysts have achieved acceptably good ethylene selectivity in the ethane ODH; this is mainly due to the ability of isolated vanadium species to provide lattice oxygen for hydrogen removal from alkanes yielding olefins via redox cycle. According to the literature data, formation of poly vanadate decreases the ethane conversion. Obviously, the ratio of V-O-V/V-O-S depends on the vanadium dispersion [38]. The uniform dispersion of active phase on the support covered the acidic and basic sites properly and impressed the activity and selectivity [39,40]. The suitable titration of acid sites by vanadium increases selectivity and, on the other hand, makes easier the access to the active sites. According to Fig. 7, the extent of sulfur anion in the V_2O_5/MgO-ZrO_2 (S1) and V_2O_5/MgO-ZrO_2 (S2) is approximately twice and quadruple of V_2O_5/MgO-ZrO_2 (S0.5) respectively, which proves the accuracy of synthesizing of catalysts.

1-4. BET Analysis

Fig. 8 shows the surface area of nanocatalysts sulfated by different concentrations of sulfuric acid. A drastically higher surface area was observed upon sulfidation using sulfuric acid compared to the non-sulfated zirconia. Deshmane et al. [35] applied TGA-DSC for zirconia and sulfated zirconia with different digestion times; they concluded that sulfidation of catalysts postponed the crystallization temperature and so increased the surface area of catalysts. According to literature, incorporation of SO_4^{-2} ions in the metal oxides cluster impresses the phase transition from crystallized to the amorphous ones. By increasing the concentration of sulfate ions, the resistance of catalysts to the transitions increases. As mentioned in the sulfidation mechanism section, in the first steps of sulfated zirconia preparation, Zr $(OH)_4$ is formed. Deshmane et al. [35] stated that by increasing the digestion time the condensation of hydroxyl groups increases, leading to the polym-

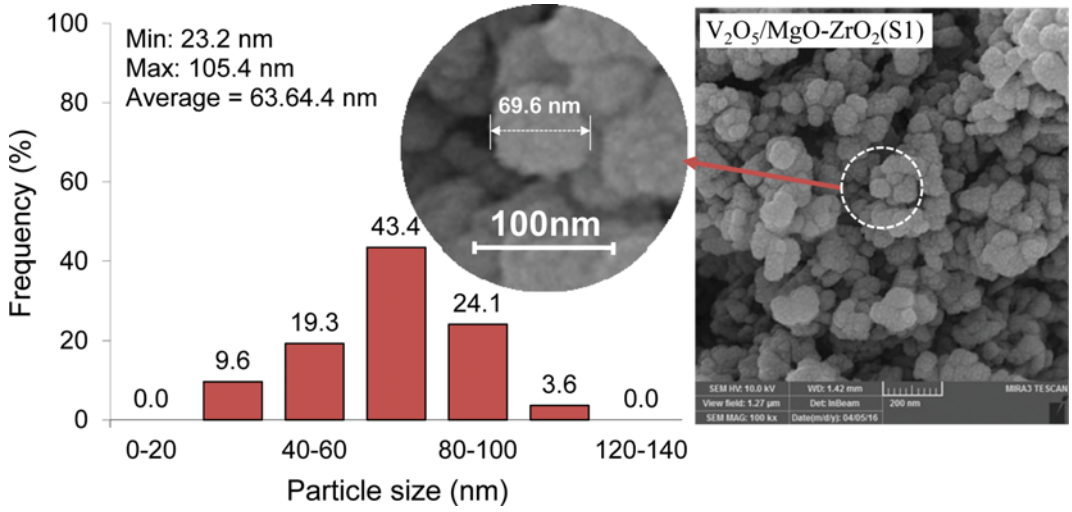

Fig. 6. Surface particle size distribution histogram of synthesized V_2O_5/MgO-ZrO_2 nanocatalysts: V_2O_5/MgO-ZrO_2(S1).

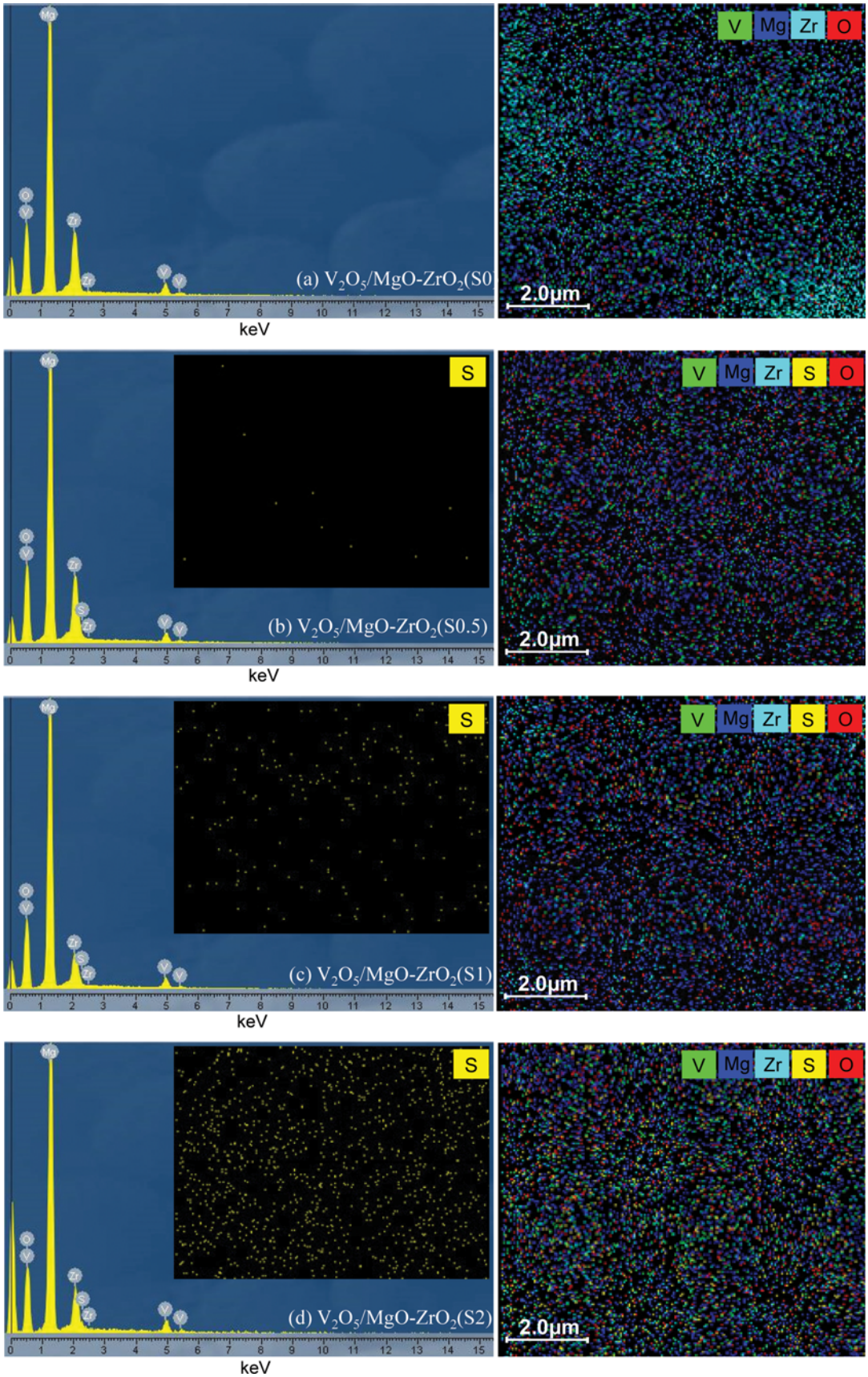

Fig. 7. EDX analysis of synthesized V_2O_5/MgO-ZrO_2 nanocatalysts: (a) V_2O_5/MgO-ZrO_2(S0), (b) V_2O_5/MgO-ZrO_2(S0.5), (c) V_2O_5/MgO-ZrO_2(S1), and (d) V_2O_5/MgO-ZrO_2(S2).

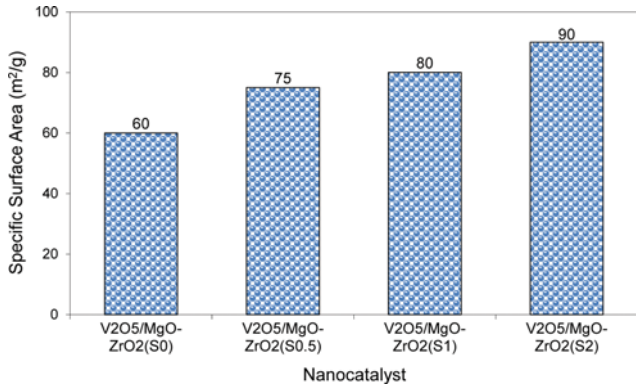

Fig. 8. BET specific surface area analysis of synthesized V_2O_5/MgO-ZrO_2 nanocatalysts.

erization, and a material with three-dimensional porous structure is formed. Obviously in our work, the concentration of sulfating agent plays the role of digestion time. The key factor in the sulfidation process is that the sulfidation of amorphous zirconia hydroxide exhibits higher surface area compared to the ones sulfated after calcination.

1-5. FTIR Analysis

Fig. 9 shows the FTIR spectra for the V_2O_5/MgO-ZrO_2 (Sx) nanocatalyst prepared by different molarities of sulfating agent. These spectra have been recorded in the range of 400-4,000 cm^{-1} wave number. The peaks in the range of 400-900 cm^{-1} are ascribed to vibrations of metal oxide bonds [41]. In the FTIR spectra of all

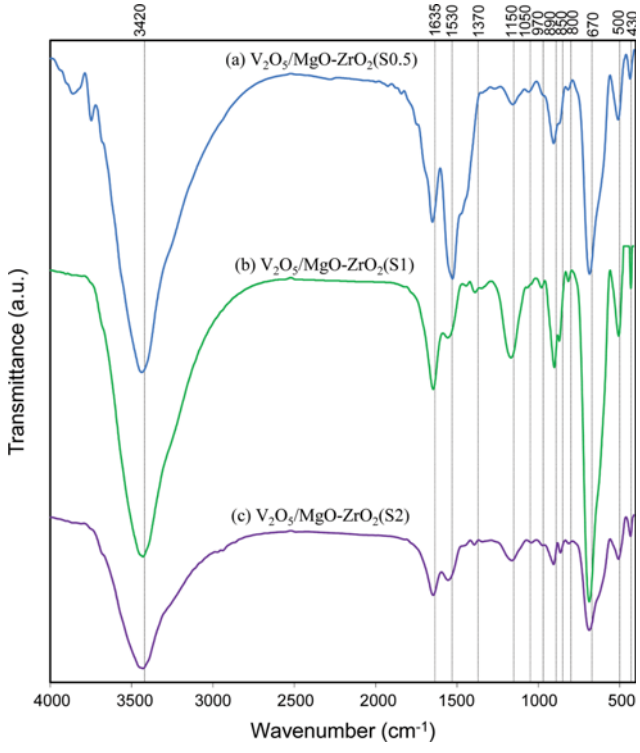

Fig. 9. FTIR spectra of synthesized V_2O_5/MgO-ZrO_2 nanocatalysts: (a) V_2O_5/MgO-ZrO_2(S0.5), (b) V_2O_5/MgO-ZrO_2(S1) and (c) V_2O_5/MgO-ZrO_2(S2).

catalysts, due to the hydration, a strong and broad band in the 3,000-3,600 cm^{-1} regions is observed related to physisorbed and/or possibly coordinated water [42-45]. According to the literature data, the active sites for oxidative dehydrogenation of alkanes are either free or bridging hydroxyl groups [46,47]. Therefore, it can be concluded that the catalysts with more intense bonds at 3,600 cm^{-1} are more active in the ODH of ethane [48]. This bond is more intense in the V_2O_5/MgO-ZrO_2 (S1) compared to the other nanocatalysts. It is expected that V_2O_5/MgO-ZrO_2 (S1) exhibits superior activity in ethane ODH. On the other hand, the hydroxyl groups prevent the formation of coke. The bonds observed close to 1,620 cm^{-1} are assigned to the bending mode (δ_{HOH}) of coordinated molecular water associated with the sulfate group. The band observed at ~970 cm^{-1} can be related to the symmetric vibrations of S-O bond while 1,050 and 1,150 cm^{-1} peaks are attributed to asymmetric stretching frequencies of O-S-O bonds [49,50]. It was pointed out that the existence of covalent S=O bonds in sulfur complexes formed on metal oxides was necessary for the generation of acidic sites. The peaks around 1,370 cm^{-1} are attributed to the stretching vibration of S=O bonds [51]. As can be seen, by increasing S content the intensity of this peak increased. These data indicated that molarity of acid has a significant effect on the nature of bonding of sulfate ions with the zirconia surface.

2. Catalytic Performance of V_2O_5/MgO-ZrO_2 Toward Ethane to Ethylene

2-1. C_2H_6 Conversion

The oxidative dehydrogenation of ethane with CO_2 from 600-700 °C is drawn in Fig. 10 for synthesized V_2O_5/MgO-ZrO_2 (Sx) nanocatalysts with different concentrations of sulfating agent. As can be seen, the ethane conversion increases by temperature for all synthesized samples due to the endothermic nature of ethane ODH by CO_2. Moreover, by increasing sulfur content, the ethane conversion increases. As reported, acid sites are needed for the activation of ethane [52-54]. In comparison, the ethane conversion is enhanced (38%) by sulfidation of zirconia by H_2SO_4. The first C-H bond cleavage occurred on the acidic sites. It is obvious that the acidity of catalyst increases by increasing of sulfur onions bonded to the zirconia. This statement is in full compliance with FTIR analy-

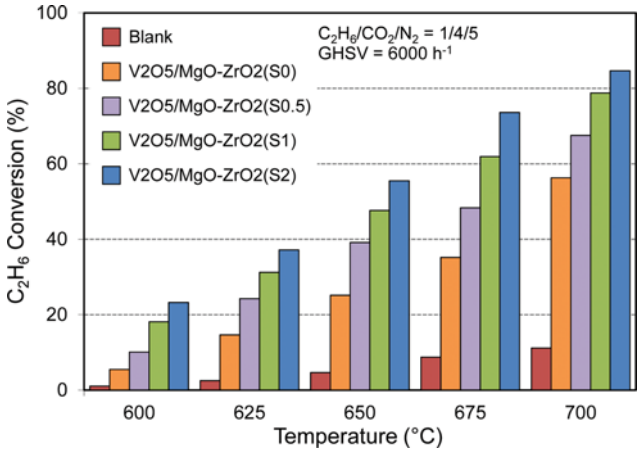

Fig. 10. C_2H_6 conversion over synthesized V_2O_5/MgO-ZrO_2 nanocatalysts at various temperatures.

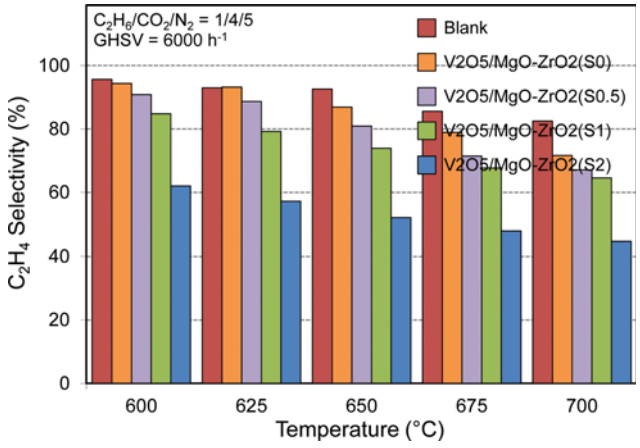

Fig. 11. C_2H_4 selectivity over synthesized V_2O_5/MgO-ZrO_2 nanocatalysts at various temperatures.

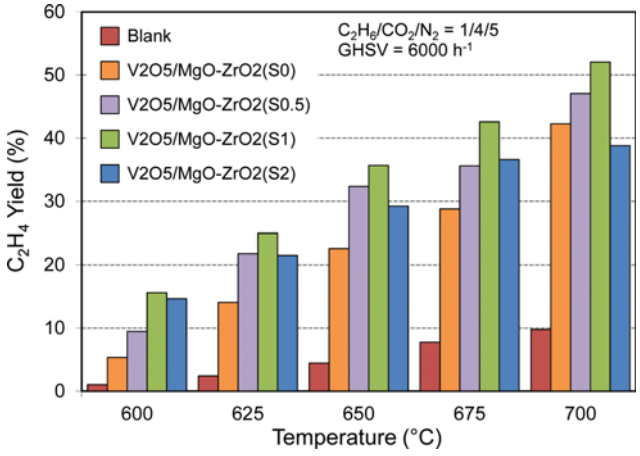

Fig. 12. C_2H_4 yield over synthesized V_2O_5/MgO-ZrO_2 nanocatalysts at various temperatures.

sis that the intensity of peaks related to the S=O increases with sulfur content.

2-2. C_2H_4 Selectivity

The ethylene selectivity of various as synthesized catalysts is shown in Fig. 11. As can be seen, the ethylene selectivity is decreased by temperature. As temperature increases, the contribution of side reaction increases as well. The activation of paraffin is harder than that of other hydrocarbons due to the high stability of the paraffin. Therefore, the products formed may be readily oxidized under the conditions required to activate paraffin, thus limiting selectivity. The extent of ethylene selectivity step downing by temperature enhancement is related to the strength of acid sites of catalysts. Moderate acidity of catalysts is commonly accepted as a crucial factor for achieving acceptable ethylene selectivity. In this case, superior surface acidity for V_2O_5/MgO-ZrO_2 (S2) and V_2O_5/MgO-ZrO_2 (S1) in spite of V_2O_5/MgO-ZrO_2 (S0.5) and V_2O_5/MgO-ZrO_2 (S0) is a noticeable factor contributing to their higher conversion of ethane. However, it has been also well known that stronger surface acidity usually exhibits undesired side-reactions, such as cracking and coking. Due to its highest acid site density, cracking is noticeable for V_2O_5/MgO-ZrO_2 (S2). On the other hand, the existence of moderate surface acid site density for V_2O_5/MgO-ZrO_2 (S0) in contrast to other synthesized nanocatalyst may well account for its clearly superior selectivity to ethylene. In the case of catalysis with basic sites, the formed olefins desorb rapidly from the surface of catalysis, and the combustion and the other reactions limited selectivity does not take palace. The results shown in Fig. 11 reveal that sulfating agent concentration biases the ethylene selectivity. It is obvious that the strength of acid sites proliferates by concentration of H_2SO_4.

2-3. C_2H_4 Yield

Fig. 12 exhibits ethylene yield on the as-synthesised nanocatalysts in the range of 600-700 °C. The results illustrated in the figure reveal that by increasing H_2SO_4 concentration, the ethylene yield increases and reaches its maximum for the V_2O_5/MgO-ZrO_2 (S1). Further increasing of sulfating agent concentration leads to a decrease in the ethylene yield. The affinity between ethane and active sites determines the ethylene productivity. The interaction between catalyst and hydrocarbons is related to the acid-base property, surface of metal oxide and vanadium dispersion. According to the literature [55] data, the electron density and the cation size specify the strength of acid sites. The more oxidized cation provides more acidic sites and inversely the cation with low density of electrical charge is known as basic sites. Busca et al. [56] calculated the charge of most active H atoms of hydrocarbons. They concluded that alkanes which are heavier than ethane have negative charge on H atom; thus, acidic sites are favorable for the dehydrogenation process. In the case of ethane, H atom of C-H bond has nearly positive charge. But there are inconclusive data in the literature about the nature of acidic or basic site required for ethane activation. In this study, the results of ethane conversion section indicate that by the enhancement of acidity of the catalyst, activity of the dehydrogenation increased; on the other hand, by increasing sulfating agent molarity used in catalysis preparing the selectivity of ethylene decreased. From the above results, we propose that in the case of vanadium supported on the MgO-ZrO_2 (Sx) nanocomposites, acidic sites are required for ethane conversion, but more basic sites are needed for ceasing of over oxidation reaction, which limits selectivity. Note that ethylene yield over V_2O_5/MgO-ZrO_2 (S1) nanocatalysts is 52% at 700 °C, which is higher than the other studied catalysts. This is due to better acid base property, well defined and uniform morphology.

2-4. Effect of O_2 Addition

To specify the contribution of O_2 to the reaction, the ethane dehydrogenation in the presence of CO_2 was compared with that condition which CO_2 and O_2 utilized simultaneously as oxidant at 650 °C over V_2O_5/MgO-ZrO_2(Sx); the results are shown in Fig. 13. The ethane conversion and ethylene yield on the V_2O_5/MgO-ZrO_2 (Sx) catalyst in the presence of O_2 is higher than that in the presence of only CO_2, boding the promoting effects of O_2 for the oxidative dehydrogenation of ethane. For the V_2O_5/MgO-ZrO_2 (S1) nanocatalyst the ethane conversion and ethylene yield in the presence of O_2 increased 47% and 15%, respectively, while ethylene selectivity decreased approximately 24%. The activation of oxidant depends on its nature and is one of the key steps in proceeding ODH reaction. The activity of CO_2 is low and its activation is nearly hard

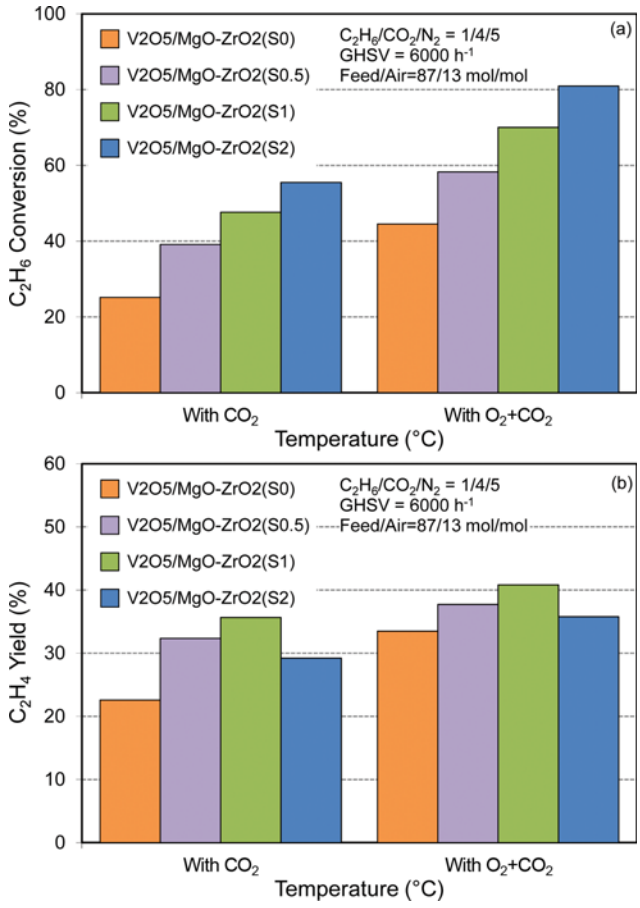

Fig. 13. CO_2 vs. O_2 oxidative dehydrogenation of ethane to ethylene over synthesized V_2O_5/MgO-ZrO_2 nanocatalysts: (a) C_2H_6 conversion and (b) C_2H_4 yield.

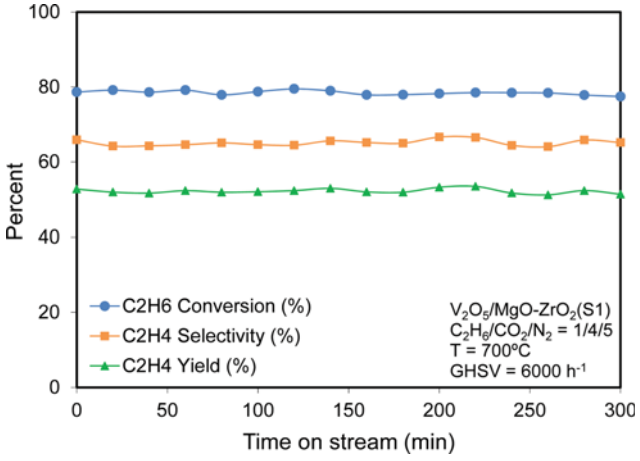

Fig. 14. Time on stream behavior of V_2O_5/MgO-ZrO_2(S1) nanocatalyst in oxidative dehydrogenation of ethane to ethylene by carbon dioxide.

and needs higher temperatures. Compared to CO_2, O_2 is activated at lower temperatures. In the case of our study, the presence of vanadium as a reducible metal oxide accelerated the O_2 activation at lower temperatures. Moreover, by comparing two cases, ethylene selectivity is higher in the absence of O_2. Thus, CO_2 is less aggressive than O_2, so the occurrence of side reactions is limited by utilization of only CO_2. Regarding the high heat capacity of CO_2, it could reduce the probability of hot spot formation [57]. It is believed that these spots are responsible for the overoxidation reaction, which lowers the ethylene selectivity. As mentioned above, by applying suitable proportion of O_2 and CO_2, one can overcome the dangers related to O_2 and lower activity pertinent to CO_2.

2-5. Time on Stream Performance

The catalytic activity of V_2O_5/MgO-ZrO_2 (S1) sample was tested for 300 min time on-stream, and the results are shown in Fig. 14. According to the ethylene yield data, maximum amount of ethylene was produced at 700 °C; thus, this temperature was selected for the investigation of deactivation of V_2O_5/MgO-ZrO_2 (Sx) nanocatalyst. As can be seen, the conversion, selectivity and ethylene yield remained constant after 6 h. These results indicate that V_2O_5/MgO-ZrO_2 (S1) is an active and stable catalyst for ethane ODH. This could be due to the proper acidity and Mg/Zr ratio utilized for the nanocatalyst preparation. On the other hand, the presence of ZrO_2 in the support reinforces the thermal stability of catalysts. The deactivation of ethane ODH catalysts mainly takes place due to the coke formation or diminishing of redox species. According to the FTIR results, existence of very intense peaks is related to the OH groups, which prevents coke formation. On the other hand, the surface area of prepared nanocatalysts is high enough to disperse vanadium properly and rule up the coke formation.

3. Reaction Mechanism of Ethane to Ethylene

A reaction mechanism for ODH of ethane was suggested; a schematic diagram of this mechanism is shown in Fig. 15. It is obvious that the adsorption of reactant on the surface of catalysis is the beginning step of all catalytic processes. Ethane could be adsorbed on the O (a) and O (b) sites of V_2O_5 supported catalysts. Fu et al. [58] concluded that the adsorption of alkanes on the O (b) sites is much stronger than on the O (a). The first C-H bonds of alkanes could be dissociated hemolytically or heterogeneously. The heterolytic cleavage of C-H bonds taking place on the surface possesses strong acid-base pairs. The products of this dissociation are ethyl radical and a proton, while the heterogeneous dissociation was done on the surface oxygen sites.

Chen et al. [59] proposed a model for activation of C-H bond that only lattice oxygen contributes without the aim of vanadium atom. According to the reaction which is given below, Fu et al. [58] attributed a mechanism in which vanadyl groups play an important role.

$$C_2H_5\text{-}H+V=O \leftrightarrow HV=OC_2H_5 \quad (3)$$

$$C_2H_5\text{-}H+V=O \leftrightarrow C_2H_5V=OH \quad (4)$$

They claimed that reaction (3) requires high energy and the products of reaction (4) are not stable. These restrictions make the occurrence of heterogeneous cleavage of C-H bond unlikely. The hemolytic dissipation of C-H bond is explained by reaction (5)

$$C_2H_5\text{-}H+O+O \leftrightarrow HO+OC_2H_5 \quad (5)$$

Two lattice oxygens are involved in this reaction. Three different paths are included in reaction (5):

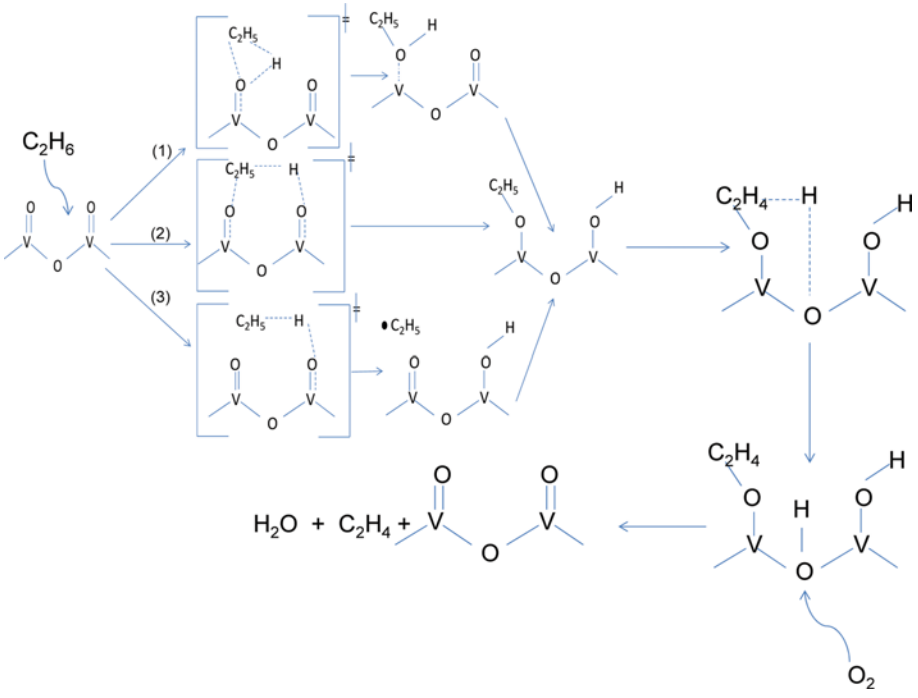

Fig. 15. Reaction mechanism of CO_2/O_2 dehydrogenation of ethane to ethylene over $V_2O_5/MgO\text{-}ZrO_2$ nanocatalyst.

i. Formation of alcohol via the reaction of O atoms with C-H bonds and at the next step, proton of alcohol migrates to the neighbor lattice oxygen.

ii. Ethane simultaneously reacts with two lattice oxygen.

iii. Similar to path 1, this is a two-step mechanism.

In the first step lattice oxygen abstracts one H atom; and then the formed ethyl groups are released to the gas phase and finally react with the other lattice oxygen. In the hemolytic dissociation of C-H bond, three types of oxygen and three different mechanisms are applicable. Since the cleavage of C-H bond via O (c) produces unstable intermediates, this site is emitted from the mechanism investigation. Bader et al. computed the net charge distributed on the O (a), O (b) and O (c) and found that the higher reducibility is a concern to the O (a) sites. On the other hand, it seems that O (b) has better contact with C-H bond compared to O (a) [60]. Because O (b) is linked to more species than O (a), the electrons concentrated on these nearby atoms could help in the activation of C-H bonds. As mentioned, the reducibility of O (a) site is more than O (b). Mechanism 1 requires more reducible sites compared to 3. Therefore, it is concluded that O (a) is favorable for both mechanisms, while on the O (b) only mechanism 3 is viable.

At the next step, the adsorbed ethoxide should be converted to ethylene. This step takes place on the O (b) sites where the neighboring oxygen adsorbs the second H atom.

CONCLUSIONS

Interesting effects of various contents of SO_4^{-2} ion introduction to the $MgO\text{-}ZrO_2$ combined support were investigated. The results confirmed that SO_4^{-2} ion changed the support character and activity in the ethane oxidative dehydrogenation to ethylene. The monoclinic phase of zirconia approximately disappeared after sulfidation of the $MgO\text{-}ZrO_2$ combined support. Also, the crystallinity of tetragonal phase of ZrO_2 decreased by increasing the sulfur content used for $MgO\text{-}ZrO_2$ (Sx) preparation. On the other hand, the introduction of SO_4^{-2} ion led to the formation of three-dimensional porous structures and enhanced the surface area of nanocatalysts and impressed the interaction between support and active phase and dispersion of vanadium. The FTIR results revealed the S=O bonds, which indicate the acidity of nanocatalysts, increased by increasing sulfur content of support. The uniform and small particle size was observed for $V_2O_5/MgO\text{-}ZrO_2$ (S1). Among the studied nanocatalysts, $V_2O_5/MgO\text{-}ZrO_2$ (S1) showed superior catalytic activity at 700 °C giving 52.03% ethylene yield due to uniform morphology, small particle size and suitable acid-base property.

ACKNOWLEDGEMENTS

The authors gratefully acknowledge Sahand University of Technology for the financial support of the project as well as Iran Nanotechnology Initiative Council for complementary financial support.

REFERENCES

1. H. Zhu, H. Dong, P. Laveille, Y. Saih, V. Caps and J.-M. Basset, *Catal. Today*, **228**, 58 (2014).
2. F. Yu, X. Wu, Q. Zhang and Y. Wang, *Chinese J. Catal.*, **35**, 1260 (2014).
3. J. P. Bortolozzi, T. Weiss, L. B. Gutierrez and M. A. Ulla, *Chem. Eng. J.*, **246**, 343 (2014).
4. A. Talati, M. Haghighi and F. Rahmani, *RSC Adv.*, **6**, 44195 (2016).
5. F. Rahmani, M. Haghighi and M. Amini, *J. Ind. Eng. Chem.*, **31**,

142 (2015).
6. F. Rahmani and M. Haghighi, *Korean J. Chem. Eng.*, **33**, 2555 (2016).
7. F. Rahmani and M. Haghighi, *J. Natural Gas Sci. Eng.*, **27**, Part 3, 1684 (2015).
8. P. Delir Kheyrollahi Nezhad, M. Haghighi, N. Jodeiri and F. Rahmani, *J. Sol-Gel Sci. Technol.*, **80**, 436 (2016).
9. E. Asghari, M. Haghighi and F. Rahmani, *J. Mole. Catal. A: Chem.*, **418-419**, 115 (2016).
10. S. Shylesh and A. P. Singh, *J. Catal.*, **233**, 359 (2005).
11. E. V. Kondratenko, O. Ovsitser, J. Radnik, M. Schneider, R. Kraehnert and U. Dingerdissen, *Appl. Catal. A: Gen.*, **319**, 98 (2007).
12. S. Sokolov, M. Stoyanova, U. Rodemerck, D. Linke and E. V. Kondratenko, *J. Catal.*, **293**, 67 (2012).
13. Z. Zhang, L. Han, R. Chai, Q. Zhang, Y. Li, G. Zhao, Y. Liu and Y. Lu, *Catal. Commun.*, **88**, 90 (2017).
14. M. P. Casaletto, L. Lisi, G. Mattogno, P. Patrono, G. Ruoppolo and G. Russo, *Appl. Catal. A: Gen.*, **226**, 41 (2002).
15. P. Ciambelli, P. Galli, L. Lisi, M. A. Massucci, P. Patrono, R. Pirone, G. Ruoppolo and G. Russo, *Appl. Catal. A: Gen.*, **203**, 133 (2000).
16. R. Gounder and E. Iglesia, *J. Catal.*, **277**, 36 (2011).
17. M. P. Casaletto, L. Lisi, G. Mattogno, P. Patrono and G. Ruoppolo, *Appl. Catal. A: Gen.*, **267**, 157 (2004).
18. G. Tanimu, B. R. Jermy, S. Asaoka and S. Al-Khattaf, *J. Ind. Eng. Chem.*, **45**, 111 (2017).
19. A. H. Elbadawi, M. S. Ba-Shammakh, S. Al-Ghamdi, S. A. Razzak, M. M. Hossain and H. I. de Lasa, *Chem. Eng. Res. Design*, **117**, 733 (2017).
20. J. Camacho-Bunquin, P. Aich, M. Ferrandon, A. "Bean" Getsoian, U. Das, F. Dogan, L. A. Curtiss, J. T. Miller, C. L. Marshall, A. S. Hock and P. C. Stair, *J. Catal.*, **345**, 170 (2017).
21. R. Khoshbin and M. Haghighi, *Catal. Sci. Technol.*, **4**, 1779 (2014).
22. M. Piumetti, B. Bonelli, M. Armandi, L. Gaberova, S. Casale, P. Massiani and E. Garrone, *Micropor. Mesopor. Mater.*, **133**, 36 (2010).
23. I. Rossetti, L. Fabbrini, N. Ballarini, C. Oliva, F. Cavani, A. Cericola, B. Bonelli, M. Piumetti, E. Garrone, H. Dyrbeck, E. A. Blekkan and L. Forni, *J. Catal.*, **256**, 45 (2008).
24. J. M. Lopez Nieto, R. Coenraads, A. Dejoz, M. I. Vazquez, S. T. O. A. M. G. R. K. Grasselli and J. E. Lyons, The role of metal oxides as promoters of V2O5/Î³-Al2O3 catalysts in the oxidative dehydrogenation of propane. In *Studies in Surface Science and Catalysis*, Elsevier, **110**, 443 (1997).
25. a. B. Demirci and F. Garin, *J. Mole. Catal. A: Chem.*, **188**, 233 (2002).
26. D. Fo*f*rcaiu, J. Q. Li and A. Kogelbauer, *J. Mol. Catal. A: Chem.*, **124**, 67 (1997).
27. H. Lee, J. K. Lee, U. G. Hong, Y. Yoo, Y.-J. Cho, J. Lee, H.-S. Jang, J. C. Jung and I. K. Song, *J. Ind. Eng. Chem.*, **18**, 808 (2012).
28. G. Chen, C.-Y. Guo, H. Qiao, M. Ye, X. Qiu and C. Yue, *Catal. Commun.*, **41**, 70 (2013).
29. M. Bensitel, O. Saur, J. C. Lavalley and B. A. Morrow, *Mater. Chem. Physics*, **19**, 147 (1988).
30. A. Corma, V. Fornos, M. I. Juan-Rajadell and J. M. L. Nieto, *Appl. Catal. A: Gen.*, **116**, 151 (1994).
31. K. Arata and M. Hino, *Appl. Catal.*, **59**, 197 (1990).
32. K. Arata, H. Matsuhashi, M. Hino and H. Nakamura, *Catal. Today*, **81**, 17 (2003).
33. C. Morterra, G. Cerrato and F. Pinna, *Spectrochim. Acta, Part A: Molecular and Biomolecular Spectroscopy*, **55**, 95 (1998).
34. G. Martra, F. Arena, S. Coluccia, F. Frusteri and A. Parmaliana, *Catal. Today*, **63**, 197 (2000).
35. V. G. Deshmane and Y. G. Adewuyi, *Fuel*, **107**, 474 (2013).
36. K. Tanabe, T. Yamaguchi and T. Inui, Design of Sulfur-Promoted Solid Superacid Catalyst, In *Studies in Surface Science and Catalysis*, Elsevier, **44**, 99 (1989).
37. A. Corma, *Chem. Rev.*, **95**, 559 (1995).
38. I. E. Wachs, J.-M. Jehng, G. Deo, B. M. Weckhuysen, V. V. Guliants, J. B. Benziger and S. Sundaresan, *J. Catal.*, **170**, 75 (1997).
39. J. Le Bars, J. C. Vedrine, A. Auroux, S. Trautmann and M. Baerns, *Appl. Catal. A: Gen.*, **88**, 179 (1992).
40. T. Blasco, A. Galli, J. M. Lopez Nieto and F. Trifiro, *J. Catal.*, **169**, 203 (1997).
41. D. Dhak and P. Pramanik, *J. American Ceramic Soc.*, **89**, 1014 (2006).
42. F. Rahmani, M. Haghighi, Y. Vafaeian and P. Estifaee, *J. Power Sources*, **272**, 816 (2014).
43. S. Khajeh Talkhoncheh and M. Haghighi, *J. Natural Gas Sci. Eng.*, **23**, 16 (2015).
44. S. Aghamohammadi and M. Haghighi, *Chem. Eng. J.*, **264**, 359 (2015).
45. E. Aghaei and M. Haghighi, *Powder Technol.*, **269**, 358 (2015).
46. L. Lisi, L. Marchese, H. O. Pastore, A. Frache, G. Ruoppolo and G. Russo, *Topics in Catalysis*, **22**, 95 (2003).
47. L. Marchese, A. Frache, G. Gatti, S. Coluccia, L. Lisi, G. Ruoppolo, G. Russo and H. O. Pastore, *J. Catal.*, **208**, 479 (2002).
48. M. A. Goula, A. A. Lemonidou and A. M. Efstathiou, *J. Catal.*, **161**, 626 (1996).
49. G. D. Yadav and J. J. Nair, *Micropor. Mesopor. Mater.*, **33**, 1 (1999).
50. K. Saravanan, B. Tyagi and H. C. Bajaj, *Catal. Sci. Technol.*, **2**, 2512 (2012).
51. M. Ejtemaei, A. Tavakoli, N. Charchi, B. Bayati, A. A. Babaluo and Y. Bayat, *Adv. Powder Technol.*, **25**, 840 (2014).
52. A. Talati, M. Haghighi and F. Rahmani, *Adv. Powder Technol.*, **27**, 1195 (2016).
53. F. Rahmani, M. Haghighi and S. Mahboob, *Ultrasonics Sonochemistry*, **33**, 150 (2016).
54. F. Rahmani and M. Haghighi, *RSC Adv.*, **6**, 89551 (2016).
55. M. A. Banares, *Catal. Today*, **51**, 319 (1999).
56. G. Busca, E. Finocchio, G. Ramis and G. Ricchiardi, *Catal. Today*, **32**, 133 (1996).
57. G. Sun, Q. Huang, S. Huang, Q. Wang, H. Li, H. Liu, S. Wan, X. Zhang and J. Wang, *Catalysts*, **6**, 1 (2016).
58. H. Fu, Z.-P. Liu, Z.-H. Li, W.-N. Wang and K.-N. Fan, *J. Am. Chem. Soc.*, **128**, 11114 (2006).
59. K. Chen, E. Iglesia and A. T. Bell, *J. Catal.*, **192**, 197 (2000).
60. W. Kutzelnigg, *Atoms in Molecules. A Quantum Theory. (Reihe: International Series of Monographs on Chemistry, Vol. 22.) Von R.F.W. Bader. Clarendon Press, Oxford, 1990. XVIII, 438 S., geb. £ 50.00. - ISBN 0-19-855168-1*. WILEY-VCH Verlag GmbH, **22**, 104 (1992).